Rational Design of Selective, Sulfur-Resistant Oxidation Emissions Catalysts

Hairong Tang and Bernhardt L. Trout*

Department of Chemical Engineering, Massachusetts Institute of Technology, 77 Massachusetts Avenue, Cambridge, Massachusetts 02139

Received: July 25, 2005; In Final Form: February 1, 2006

A new catalyst design strategy based on optimizing electronic structure has been proposed and then applied to a very important environmental application, the design of selective, sulfur-resistant oxidation emissions catalysts. The modified d-band center model developed by us in a previous study, together with an energy decomposition scheme, is used to correlate measures of reactivity with reaction barriers of $SO_2 + O \rightarrow SO_3$ and $NO + O \rightarrow NO_2$ on surfaces. Our objective is to find a catalyst which is active in oxidizing NO to NO_2 but relatively inactive in oxidizing SO_2 to SO_3. The Ir alloyed Pt(111) surface is found to have the highest selectivity for oxidation of NO over SO_2 at 700 K. Unfortunately, there is a slope change in the correlation of the weighted d-band center with the adsorption of NO at the transition state, which narrows down the range of the theoretical selectivity. Our ongoing study aims at understanding the reason for this. The general importance of this study for surface catalysis is also discussed.

1. Introduction

Three-way catalysts (TWCs), consisting of platinum, palladium, rhodium, and other components, are widely used for exhaust aftertreatment in automobiles. They operate by simultaneously reducing nitrogen oxides (NO_x) and oxidizing the partial combustion product (CO) and the residual uncombusted hydrocarbons (HC). To both reduce and oxidize effectively, they can operate only within a very narrow window around the stoichiometric value of the air−fuel ratio (~14.7).[1] However, it is highly desirable to have emissions catalysts that operate under lean (oxygen rich) conditions. Such catalysts could be used for emissions control of diesel engines and of gasoline engines that burn under lean conditions, with the latter being useful for increased fuel economy and control range. Thus, the main challenge for controlling emissions under lean conditions is to remove adequately the oxides of nitrogen from exhaust streams that contain a large excess of oxygen, because, under these conditions, the conversion efficiency for the reduction reaction of NO_x is low. Possible ways to overcome this difficulty include selective catalytic reduction (SCR), in which a reductant such as urea or ammonia is added to react preferentially with the oxygen from the NO_x,[2] and lean NO_x trapping, in which NO_x is stored on a trap (such as BaO or CaO) for a period of lean operation, followed by a short period of rich operation, in which stored NO_x is converted to N_2 and purged.[3] Both of these, especially the latter one, are poisoned by sulfur compounds from the fuel. In the case of the NO_x trap, the oxidizing component (typically Pt) also promotes the oxidation of SO_2 to SO_3 under lean conditions. SO_3 then adsorbs strongly on the NO_x trap and forms thermodynamically stable sulfates, such as $BaSO_4$, which are very hard to purge and which thus deactivate the trap. Solutions for this problem include reducing the amount of sulfur in the fuel or designing new sulfur-resistant catalysts which are selective in the oxidation of NO over SO_2. In this paper, we will focus on the latter one: the design of selective, sulfur-resistant catalysts.

Alloying metals has long been exploited as an effective way to enhance the reactivities of surfaces via either the electronic effect or the ensemble effect or both.[4] The electronic effect is due to a change in electronic structure, leading to a change in rate constants of elementary steps, while the ensemble effect is due to a change in distribution and availability of surface reaction sites. So far, most heterogeneous catalysts are developed using heuristics and trial-and-error methods via continual incremental improvements of existing catalysts or via a combinatorial approach. Incremental improvements are made by modifying existing catalysts and then testing them empirically until better catalysts are found. The TWCs discussed in the last paragraph are one of the great successes of this kind of catalyst development. They have been continuously improved since the 1970s. In the combinational approach, a large number of catalyst formulations are synthesized and tested rapidly, for example, via high-throughput screening, to optimize catalyst properties. Both approaches are limited by the efficiency of exploring the huge possible parameter space. It would be desirable to be able to propose a priori more limited ranges of compositions to explore.

We use a different approach, called rational catalyst design, based on the relationships between the intrinsic properties of materials and their catalytic activities, the latter being obtained via electronic structure theories of chemical binding and reactivity. A very successful example of this approach is the design of a noncoking steam reforming catalyst by Besenbacher et al.[5] This catalyst design was based on the ensemble effect, adding a dopant to the surface to prevent nucleation of carbon material without affecting the activity for steam reforming. Obviously, this approach can save significant cost and time in finding new catalysts.

In this paper, we propose and apply a selective catalyst design strategy based on the electronic effect for oxidation catalysts, with a view to the reduction of emissions from automobile sources. The d-band center weighting model by Tang et al., proven to be suitable for the binding of chemisorbed molecules which bind unequally to multiple types of surface atoms,[6,7] is

* To whom correspondence should be addressed. E-mail: trout@mit.edu.

10.1021/jp054112u CCC: $33.50
Published on Web 03/11/2006

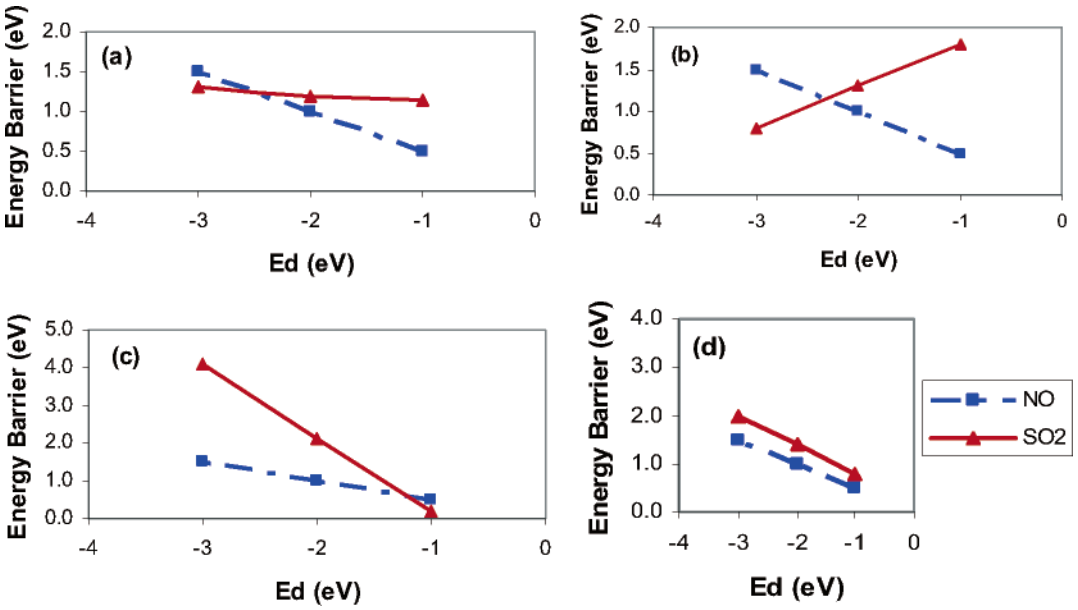

Figure 1. Illustration of possible cases of the energy barrier vs d-band center, E_d, for NO oxidation (dashed line) and SO_2 oxidation (solid line).

used together with a scheme for decomposing energies of adsorption and reaction barriers on surfaces[8,9] in order to predict the reactivity of SO_2 and NO oxidation on different surfaces. The objective is to develop a catalyst which is selective for the oxidation of NO over SO_2. Nudged elastic band (NEB) calculations are then performed to validate our assumptions. This study should aid in the development of more effective catalysts for an extremely important environmental application. It addresses exactly the selectivity issue for the future of catalytic research in this area summarized in the review by Shelef et al.,[10] of maximum importance is "a search for catalysts active in the oxidation of NO to NO_2 and relatively inactive in the oxidation of SO_2 to SO_3".

2. Computational Details

All of the adsorption energies and reaction barriers on various surfaces were calculated by first principles density functional theory (DFT) methods, implemented in the GNU publicly licensed software DACAPO.[11] The gradient-corrected exchange-correlation functional PW91-GGA[12] was used for all of the calculations. The ionic cores were described by ultrasoft pseudopotentials,[13,14] allowing the plane-wave basis set a cutoff kinetic energy of 25 Ry (340 eV). A Monkhorst−Pack mesh with a $4 \times 4 \times 1$ *k*-grid was applied to sample the surface Brillouin zones.[15] All of the surfaces were modeled by a (2×2) unit cell and periodic three-layer slabs separated by a vacuum region of ~10 Å. There might be possible lateral interactions introduced by using a (2×2) unit cell. (In our previous study,[16] the SO_3 adsorption energy difference between (2×2) and (3×3) was about 25 kJ/mol.) The nonphysical dipole interactions among slabs in the *z* direction (the direction perpendicular to the slabs) were annihilated by the self-consistently generated external dipole layer located in the middle of the vacuum. The feasibility of applying this slab model to describe accurately the adsorption properties has been tested thoroughly by previous studies by our group and others.[6,7,9,16−24] The adsorbates and the first two-layer metal surface atoms in the slab were allowed to relax during the calculations, with the bottom Pt layer being fixed at the calculated bulk lattice constant, 4.00 Å. Taking electron spin into account explicitly was found not to change the adsorption energies of either SO_x or NO_x significantly (including adsorption on Ni).[6,8,16,20,25−27] Therefore, all of the calculations were nonmagnetic in this study.

Consistent with our previous two papers,[6,7] $n\mathrm{M}^x$/Pt(111) is used to designate the surface alloys and overlayers, meaning to replace *n* Pt atoms in the top Pt layer with other metal atoms (M). $n = 1$, 2, or 3 are surface alloys with different local concentrations of M, such that $n = 4$ is an overlayer; *x* represents the sites replaced among those four consisting of the $p(2 \times 2)$ unit cell.

The Nudged elastic band (NEB) method[28,29] was used to determine the minimum energy path (MEP) connecting the initial and final states. The transition state of the reaction corresponds to the saddle point along this path. The NEB method determines the MEP by creating intermediate images along the path that represent replicas of the original system and then simultaneously relaxing them. Spring constants between the adjacent images are added to ensure the continuity of the path. Because the NEB method does not require second or higher order derivatives of the Kohn−Sham energy functional with respect to the atomic coordinates, it is particularly useful when combined with the plane-wave DFT computations. To save computational cost, we start the minimization process from the previous MEPs of reactions on clean Pt(111) surfaces[9,30] and terminate it when the nudged forces on all images of the chain becomes small (~0.07 eV/Å).

3. Results and Discussion

3.1. Strategy for Selective Catalyst Design. *3.1.1. Overall Design Strategy.* We design the selective, sulfur-resistant catalysts based on the difference of the energy barriers of $SO_2 + O \rightarrow SO_3$ and $NO + O \rightarrow NO_2$. To predict which materials will be most selective, we need a composition−activity relationship, correlating energy barriers to the intrinsic properties of the electronic structures of surfaces, such as the d-band center of metal surfaces. Energy barriers of different reactions as functions of d-band centers that illustrate possible cases which might occur are plotted in Figure 1. Dashed lines are for the oxidation of NO, and solid lines are for the oxidation of SO_2. The plot in Figure 1a shows that when the d-band center shifts toward the Fermi energy, the energy barrier for the oxidation of NO decreases much faster than that of SO_2. Since our

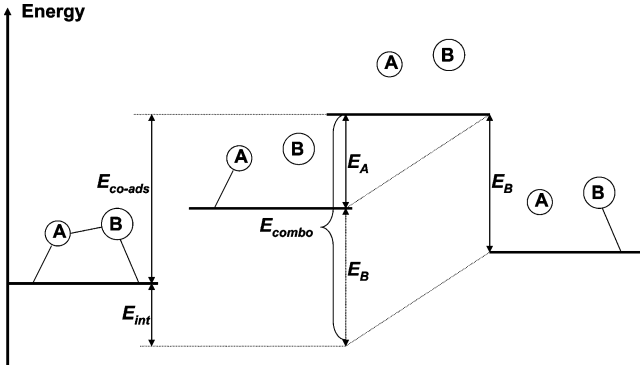

Figure 2. Energy decomposition scheme for a coadsorbed system on the surface. All of the terms are defined in the text.

objective is to activate NO oxidation, but not SO_2 oxidation, we can try to modify the surface so that the d-band center of the surface is as close to the Fermi level as possible. The energy barrier for the oxidation of NO will therefore decrease more than that of SO_2, and the selectivity will then be enhanced. The same strategy can be applied to the case illustrated in Figure 1b. Figure 1c gives an opposite case to that in Figure 1a: with the increase of the d-band center, the energy barrier for NO oxidation decreases much slower than that for SO_2 oxidation. Therefore, we need to modify the surface such that the d-band center is as far away from the Fermi level as possible. In Figure 1d, the energy barrier of NO + O → NO_2 has a similar sensitivity to the d-band center of surfaces as that of SO_2 + O → SO_3. Thus, another approach, such as exploiting the ensemble effect would need to be used. Of course, the cases in Figure 1 are merely possibilities, and the real situation may be more complicated.

3.1.2. Approach to Carry Out the Strategy. The adsorption energy of a coadsorbed system, E_{coads}, can be decomposed as (refer to Figure 2)[8,9]

$$E_{coads} = E_{combo} + E_{int} \quad (1)$$

where E_{combo} is defined as the sum of the individual energies of chemisorption of each species in the coadsorbed system (which is equivalent to the rebonding potential energy in Hammer's work)[8] and E_{int} is the intermolecular interaction energy between the individual species in the coadsorbed system. Correspondingly, the energy barrier of a reaction, E_a, can also be broken down into two contributions:[8,9]

$$E_a = \Delta E_{combo} + \Delta E_{int} \quad (2)$$

where $\Delta E_{combo} = E^{TS}_{combo} - E^{IS}_{combo}$ is the energy change in the combining potential energy of non-interacting species between the transition state geometry (TS) and the initial geometry (IS) and $\Delta E_{int} = E^{TS}_{int} - E^{IS}_{int}$ is the interaction energy change from the initial state to the transition state. Usually, for association reactions, the reactants are well separated. Liu and Hu pointed out the following:[9,31] "Generally, $E_{int} \approx E^{TS}_{int}$. This is due to the fact that the interaction energy at the initial state, E^{IS}_{int}, is usually very small at low and medium coverages". It is normally less than 0.1 eV from our calculations and reports from the literature.[9,31−33] Therefore, it is reasonable to neglect E^{IS}_{int}.

For the oxidation reactions, SO_2 + O → SO_3 and NO + O → NO_2, previous studies have reported that the rate-limiting steps in both reactions are surface reactions.[9,16] At low coverage, the Langmuir−Hinshelwood mechanism is reasonable for both reactions, in which both reactants preadsorb to surfaces before the reactions take place. Of course, if other steps are rate limiting, our catalyst design approach could be modified easily to address those steps.

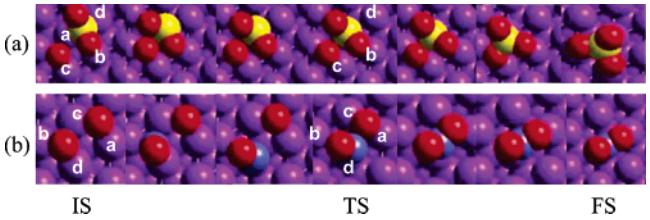

Figure 3. NEB chain images of oxidation reactions: (a) SO_2 + O → SO_3; (b) NO + O → NO_2. The first, middle, and last images in each row are the initial state (IS), the transition state (TS), and the final state (FS), respectively.

When we apply the above barrier decomposition scheme to these two oxidation reactions, we can decompose the energy barriers of those two oxidation reactions as shown below:

$$E_{oxi\text{-}SO_2} = (E^{TS}_{SO_2} - E^{IS}_{SO_2}) + (E^{TS}_{O} - E^{IS}_{O}) + E^{TS}_{int,SO_2} \quad (3)$$

$$E_{oxi\text{-}NO} = (E^{TS}_{NO} - E^{IS}_{NO}) + (E^{TS}_{O} - E^{IS}_{O}) + E^{TS}_{int,NO} \quad (4)$$

Figure 3 illustrates the minimum energy paths of both oxidation reactions on a clean Pt(111) surface, calculated by the NEB method. Those images with the $p(2 \times 2)$ unit cell marked as a, b, c, and d are at the initial state (first image of each row in Figure 3) or the transition state (fourth image of each row in Figure 3). For the surface reaction of SO_2(ads) + O(ads) → SO_3(ads), as shown in Figure 3a, both SO_2 and O start initially at face-centered cubic (fcc) sites on the surface, in the transition state, SO_2 moves to a tilted top position (site a in TS of Figure 3a) and the preadsorbed oxygen atom moves to a bridge site (between sites c and d in TS of Figure 3a) against the SO_2 molecule. This is also what our previous study found.[30] Similarly, in the reaction of NO(ads) + O(ads) → NO_2(ads) (refer to Figure 3b), both NO and O start from the fcc 3-fold hollow sites and reach a transition state which involves NO positioned just off an atop site (site d in TS of Figure 3b) with the preadsorbed oxygen atom situated on a bridge site (between sites a and c in Figure 3b). This is in agreement with Burch et al.'s study[9] in which two structures with similar energy barriers were located at transition states in which bond formation occurs across a hexagonal close-packed (hcp) or fcc hollow site. Here, we consider only the one over the hcp site. (The computation of the other possibilities is pending.) However, this will still allow us to study the trend of energy barrier change versus the electronic structure of surfaces.

Since, in both reaction paths, the preadsorbed oxygen atom moves from an fcc site in the initial state to a bridge site in the transition state, it is reasonable to assume that the combining energy change due to this preadsorbed oxygen atom in eqs 3 and 4, $E^{TS}_{O} - E^{IS}_{O}$, is similar. The interaction energy, $E^{TS}_{int,SO_2/NO}$, usually has two origins: the bonding competition effect and direct Pauli repulsion.[32] The bonding competition effect is strong when two species share bonds with the same surface atoms. In the transition states for both SO_2(ads) + O(ads) → SO_3(ads) and NO(ads) + O(ads) → NO_2(ads), the preadsorbed oxygen atom does not share bonds with either SO_2 or NO. Therefore, the contribution of bonding competition to the systems studied here is assumed to be small. The Pauli repulsion effect is short ranged and is significant only when two species are very close. The distance between SO_2 and preadsorbed oxygen in the transition state geometry of SO_2(ads) + O(ads) → SO_3(ads) is

TABLE 1: Adsorption Energies (AEs) of the Most Stable Configurations of SO_2 with Initial Geometries on Various Surface Alloys nM^x/Pt(111) and the Weighted d-Band Center, E_d, of Each Surface

nM^x/Pt(111)	AE (kJ/mol)	E_d (eV)
clean Pt(111)	−115.73	−2.55
1Pd^b/Pt(111)	−131.07	−2.39
1Pd^c/Pt(111)	−124.22	−2.44
2Pd^{bc}/Pt(111)	−139.31	−2.26
1Cu^b/Pt(111)	−142.25	−2.39
1Cu^c/Pt(111)	−143.12	−2.42
2Cu^{bc}/Pt(111)	−166.64	−2.24
1Ni^b/Pt(111)	−141.40	−2.28
1Ni^c/Pt(111)	−168.71	−2.38
2Ni^{bc}/Pt(111)	−193.83	−2.02
3Ni^{abc}/Pt(111)	−217.23	−1.71
1Ru^a/Pt(111)	−141.84	−2.46
1Ru^b/Pt(111)	−115.42	−2.60
2Ru^{ab}/Pt(111)	−145.59	−2.38
2Ru^{bc}/Pt(111)	−173.96	−2.29
2Ru^{ad}/Pt(111)	−158.29	−2.34
3Ru^{bcd}/Pt(111)	−202.22	−2.05
3Ru^{abd}/Pt(111)	−163.76	−2.15
4Ru^{abcd}/Pt(111)	−222.13	−1.79

about 2.6 Å,[30] where the Pauli repulsion is considered to be small. Although the distance between NO and preadsorbed O in the transition state of NO(ads) + O(ads) → NO_2(ads) is about 1.6 Å, $E^{TS}_{int,NO}$ is found to contribute only a small part (0.2 eV) to the energy barrier (1.52 eV).[9] Similar phenomena are also observed in the reaction of NH_2 + H → NH_3 on Rh(111).[32] This is because, in the NH_2 + H reaction, NH_2 is activated from the bridge site to just off the atop site, which costs a significant amount of energy. Also, the low coordination of NH_2 in the transition state can change the electronic distribution of NH_2. As a result, the incurred Pauli repulsion between NH_2 and H is reduced. Since the reaction of SO_2(ads) + O(ads) → SO_3(ads) is similar to the reaction of NO + O and NH_2 + H, its E^{TS}_{int,SO_2} value should not play an important role in the energy barrier. Thus, to describe the barriers in eqs 3 and 4, we can focus only on the combining energy changes for SO_2 and NO.

We are assuming that the geometries of transition states on different surface alloys do not vary dramatically from one to another. This should be valid based on studies in the literature on similar reactions. In the study of carbon monoxide oxidation on the Cu_3Pt(111) alloy surface by Zhang et al., the transition state remains similar to that on clean Pt(111) and Cu(111) surfaces.[33] The variation in the distance between the carbon atom and a surface metal atom is within 0.05 Å. More importantly, we verified this assumption via the NEB calculations in our study, to be discussed later.

Unfortunately, we cannot use a simple d-band center to describe the electronic structure of the surface for reasons described in previous studies.[6,7] We can, however, use the electronic composition−property relationship developed in a previous study, which has been successfully applied to SO_2[6] and NO[7] chemisorption on Pt(111) surfaces, alloys, and overlayers. It is used here to correlate the adsorption energies of species in the initial state and the transition state to the weighted d-band centers of the surfaces. The remaining terms in eqs 3 and 4 can then be easily estimated by only a few calculations. Finally, by examining the sensitivity difference of the energy barriers of SO_2 + O → SO_3 and NO + O → NO_2 to the weighted d-band center of surfaces, we should be able to predict which alloy surfaces will have better selectivities, as described in the previous section.

3.2. Estimation of $E^{TS}_X - E^{IS}_X$ in X + O → XO (X = SO_2 and NO). *3.2.1. $E^{IS}_{SO_2}$ and E^{IS}_{NO}.* For the reaction of SO_2 + O → SO_3, the geometries of SO_2 at the initial state on different surfaces were chosen from the most stable adsorbed configuration (fcc η^2-S_b, O_a) on the clean Pt(111) surface, determined in our previous studies.[16,30] As discussed in our previous paper,[6] the adsorption energies of the most stable configurations of SO_2 on various surface alloys were found to depend linearly on the weighted d-band centers of the surfaces. Here, the most stable configurations are defined as those for which the adsorption energy decreases as sites are substituted one at a time. This observation is used here to estimate the adsorption strength of SO_2 on surfaces with widely varying compositions. The adsorption energies of the most stable configuration of SO_2 on various surfaces (summarized in Table 1) are plotted as a function of the weighted d-band centers in Figure 4. The equation of the least-squares fitted line is

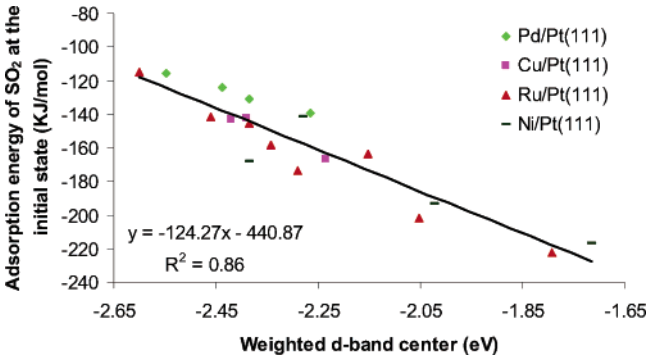

Figure 4. Linear relationship between the adsorption of SO_2 in its most stable configuration at the initial state (fcc site) on various alloyed Pt(111) surfaces and overlayers vs the weighted d-band center of the surfaces.

$$y = -124.27x - 440.87 \quad (5)$$

where y (units of kJ/mol) represents the adsorption energy of SO_2 at the initial state and x (units of eV) represents the weighted d-band center. The R^2 value of this fitted line is 0.86.

For the reaction of NO + O → NO_2, previous studies show the most stable adsorption site of NO on Pt(111) is the fcc hollow site.[7,9,19] The fcc site was therefore chosen here to be the initial position of the reactant NO on each surface. Allowing full relaxation as opposed to using the same geometry at initial state changes the energy of adsorption by only 7 kJ/mol at most. It has been shown in a previous paper of ours[7] that the adsorption energy of NO at an fcc site on Rh/Pt(111) and Pd/Pt(111) alloy surfaces has a strong linear correlation with the weighted d-band centers of surfaces calculated by our method.[6] In Figure 5, those adsorption energies on different surfaces (summarized in Table 2) are plotted versus the weighted d-band centers in the same figure. Some vacant square points marked as 1M^d/Pt(111) are added to test the generality of the linear relationship and were not used in obtaining the relationship. They will also be used to estimate the values of $E^{TS}_{NO} - E^{IS}_{NO}$ on different surfaces later. The R^2 value of the least-squares fitted line in Figure 5 is 0.90 with the correlation equation:

$$y = -159.42x - 599.34 \quad (6)$$

where y (units of kJ/mol) represents the adsorption energy of NO at an fcc site and x (units of eV) represents the weighted d-band center.

3.2.2. $E^{TS}_{SO_2}$ and E^{TS}_{NO}. The geometries of SO_2 and NO at transition states are taken and fixed from the NEB chain images at the transition states on pure Pt(111) by removing the preadsorbed oxygen atom (refer to Figure 3). At the transition

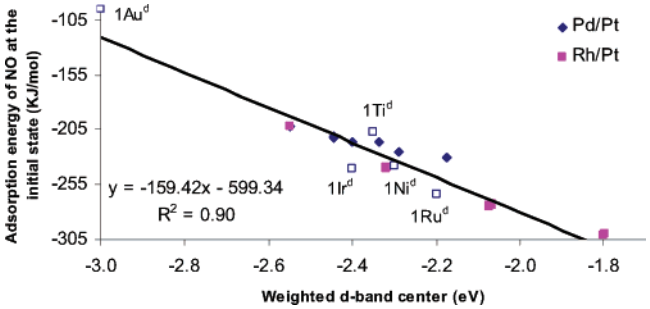

Figure 5. Linear relationship between NO adsorption at the initial state (fcc site) on various alloyed Pt(111) surfaces and overlayers vs the weighted d-band center of the surfaces. The vacant square points marked as $1M^d$/Pt(111) are added to test the generality of the linear relationship.

TABLE 2: Adsorption Energies (AEs) (Units of kJ/mol) of NO Chemisorbed on (a) Rh/Pt(111) Surfaces and (b) Pd/Pt(111) Surfaces and the Weighted d-Band Center of Each Surface, E_d (Units of eV)

(a) Rh/Pt			(b) Pd/Pt		
system	AE	E_d	system	AE	E_d
clean Pt(111)	−202.6	−2.55	clean Pt(111)	−202.6	−2.55
$1Rh^a$/Pt(111)	−240.2	−2.32	$1Pd^a$/Pt(111)	−211.5	−2.44
$1Rh^b$/Pt(111)	−240.7	−2.32	$1Pd^b$/Pt(111)	−211.9	−2.44
$1Rh^c$/Pt(111)	−201.9	−2.55	$1Pd^c$/Pt(111)	−215.9	−2.40
$1Rh^d$/Pt(111)	−240.2	−2.32	$1Pd^d$/Pt(111)	−211.3	−2.44
$2Rh^{ab}$/Pt(111)	−273.8	−2.07	$2Pd^{ab}$/Pt(111)	−216.1	−2.34
$2Rh^{ac}$/Pt(111)	−239.8	−2.32	$2Pd^{ac}$/Pt(111)	−224.8	−2.29
$2Rh^{bc}$/Pt(111)	−240.8	−2.32	$2Pd^{bc}$/Pt(111)	−225.5	−2.29
$2Rh^{ad}$/Pt(111)	−273.2	−2.07	$2Pd^{ad}$/Pt(111)	−216.6	−2.34
$2Rh^{bd}$/Pt(111)	−274.0	−2.07	$2Pd^{bd}$/Pt(111)	−216.1	−2.34
$2Rh^{cd}$/Pt(111)	−239.8	−2.32	$2Pd^{cd}$/Pt(111)	−224.8	−2.29
$3Rh^{bcd}$/Pt(111)	−275.1	−2.07	$3Pd^{bcd}$/Pt(111)	−230.3	−2.18
$3Rh^{acd}$/Pt(111)	−273.8	−2.07	$3Pd^{acd}$/Pt(111)	−230.5	−2.18
$3Rh^{abd}$/Pt(111)	−300.5	−1.80	$3Pd^{abd}$/Pt(111)	−218.4	−2.32
$3Rh^{abc}$/Pt(111)	−275.1	−2.07	$3Pd^{abc}$/Pt(111)	−230.2	−2.19
$4Rh^{abcd}$/Pt(111)	−301.4	−1.80	$4Pd^{abcd}$/Pt(111)	−232.9	−2.05

state, the correlations of the adsorption energies of SO_2 and NO on different surfaces with the weighted d-band center are plotted in Figures 6 and 7. For SO_2 at the TS, surfaces with different types and different local concentrations of alloyed species have been examined. Figure 6 shows that the adsorption strength of SO_2 at the transition state has a strong linear correlation with the weighted d-band center of each surface (R^2 = 0.94). The least-squares fitted line has the equation format as given in Figure 6:

$$y = -100.48x - 331.15 \qquad (7)$$

where y (units of kJ/mol) represents the adsorption energy of SO_2 at the transition state and x (units of eV) represents the weighted d-band center. For NO at the TS, only surfaces with single substitutions are examined. The single substitution site is chosen to be the tilted top site where NO adsorbs at the transition state. (Refer to site d in TS of Figure 3b.) This is because that is the substitution of the site where NO interacts directly, thus affecting the NO adsorption strength the most. Different from the trend observed in the other systems, such as SO_2 at the IS and at the TS and NO at the IS, Figure 7 shows that the adsorption energy of NO at the TS has a minimum as a function of the weighted d-band center. At lower values of the weighted d-band center (lower than −2.22 eV such as $1Au^d$/Pt(111), clean Pt(111), and $1Ir^d$/Pt(111)), the NO adsorption energy at the TS becomes stronger as the weighted d-band center shifts closer to the Fermi energy level. At a higher value of the weighted d-band center (higher than −2.22 eV such as $1Ru^d$/

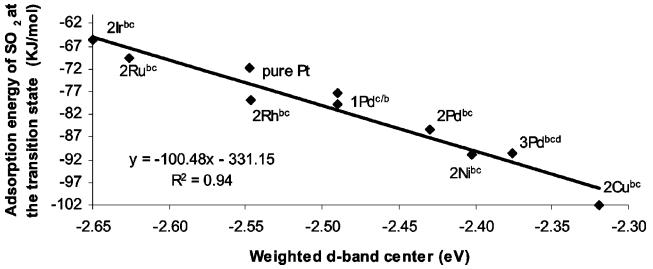

Figure 6. Linear relationship between SO_2 adsorption at the transition state on various alloyed Pt(111) surfaces and overlayers vs the weighted d-band center of the surfaces.

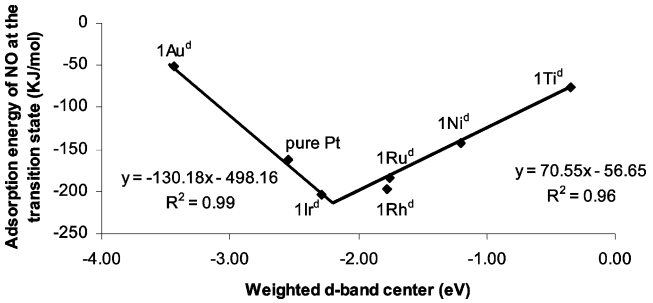

Figure 7. Linear relationship between NO adsorption at the transition state on various alloyed Pt(111) surfaces and overlayers vs the weighted d-band center of the surfaces.

Pt(111), $1Rh^d$/Pt(111), $1Ni^d$/Pt(111), and $1Ti^d$/Pt(111)), the NO adsorption energy at the TS decreases as the weighted d-band center shifts closer to the Fermi energy level. The correlation of NO adsorption energy versus weighted d-band center can be represented in the equations below:

$$y = -130.18x - 498.16 \quad (x \le -2.22 \text{ eV}) \qquad (8)$$

$$y = 70.55x - 56.65 \quad (x \ge -2.22 \text{ eV}) \qquad (9)$$

where y (units of kJ/mol) represents the adsorption energy of NO at the transition state and x (units of eV) represents the weighted d-band center.

The slope change in Figure 7 is associated with the difference in the d states of surface alloy atoms. Loffreda et al. found that the gas phase NO molecule has the electronic configuration $[1\sigma]^2[2\sigma]^2[3\sigma]^2[4\sigma]^2[1\pi]^4[5\sigma]^2[2\pi^*]^1$, where the $[2\pi^*]$ orbital is an antibonding orbital of N−O molecule, containing one electron, and all the others are fully occupied bonding orbitals.[34] The density of state (DOS) projected on the d orbitals of the surface alloy atoms and the p_x orbitals of N in NO adsorption at TS (top) on surface alloys are given in parts a and b of Figure 8, respectively, where the x axis is parallel to the surfaces. The zero on the energy axis corresponds to the Fermi level. According to Loffreda et al.'s study,[34] the peaks at a lower energy level in Figure 8b represent the mixing of 5σ and 1π orbitals, while those at a higher energy level represent $2\pi^*$ orbitals of N−O adsorbed on surfaces. In the gas phase molecule, the occupancy of the antibonding states depends on the number of electrons in the system. However, at a metal surface, there is an infinite sea of metallic electrons and the occupancy of the antibonding states (e.g., NO−M system) depends only on the energy of these states relative to the Fermi level. Because the energies of the d states relative to the Fermi level vary substantially from one metal to another (refer to Figure 8a), the number of antibonding states that are above the Fermi level, and thus empty, will depend on the metal itself. When bonding and antibonding states are formed, the strength of the bond will depend on the relative occupancy of these states.

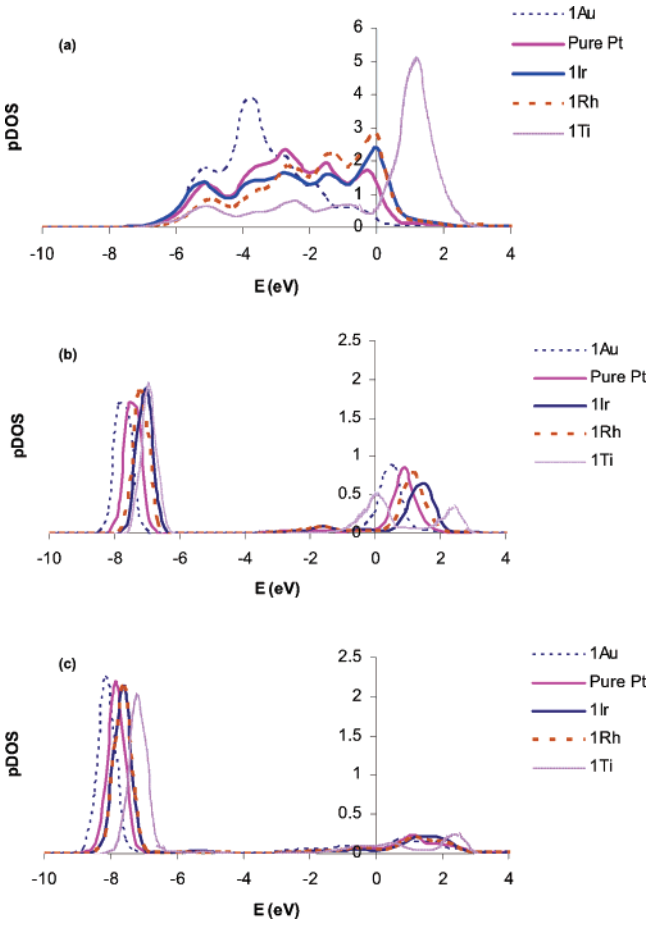

Figure 8. Local projected density of state (pDOS) of (a) d orbitals of M in $1M^d/Pt(111)$ (there is no adsorbate), (b) p_x orbitals of N for NO adsorption at TS (top) on $1M^d/Pt(111)$, and (c) p_x orbitals of N for NO adsorption at IS (fcc) on $1M^d/Pt(111)$, where M = Au, Pt, Ir, Rh, and Ti. In parts b and c, the *x* axis is defined to be parallel to the surfaces, and there is only a NO adsorbate.

If only the bonding states are filled, there will be a strong bond, whereas if the antibonding states are also filled, the bond will become considerably weaker.[35]

For example, as illustrated in Figure 8a, Au has d bands well below the Fermi level, and the antibonding states of NO on the Au alloyed surface will thus be partly below the Fermi level and filled (refer to Figure 8b). The d-contribution of Au to the NO−Au bond is therefore not attractive. This is similar to the case of N adsorbed on Cu(100) in Nilsson et al.'s work.[35] On the other hand, Pt, Ir, and Rh behave similarly to the case of Ni in Nilsson et al.'s work.[35] They have d bands partly above the Fermi level (see Figure 8a), and therefore, the antibonding states of NO on M alloyed surfaces (M = Pt, Ir, and Rh) are mostly above the Fermi level and are empty; thus, the interactions between M and NO will be much more attractive (see Figure 8b). The relative strength depends on the relative occupancy of the bonding and antibonding states. The Ir alloyed system has the lowest occupation of antibonding states, since its peak, above the Fermi level in Figure 8b, has the highest energy. Correspondingly, it also has the strongest adsorption energy of NO. Although Ti has most of its d bands above the Fermi level, as shown in Figure 8a, it still has the antibonding states of NO on the Ti alloyed surface below the Fermi level and filled (refer to Figure 8b); the strength of the interaction between NO and Ti is therefore reduced dramatically. This explains the slope change in Figure 7. Interestingly, this phenomenon does not happen when NO adsorbs at IS (fcc) (refer to Figures 5 and 8c).

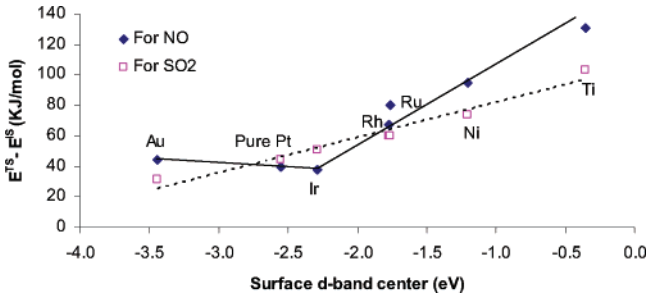

Figure 9. Correlation of the energy differences of SO_2 and NO between the initial state and the transition state on various alloyed Pt(111) surfaces ($1M^x/Pt(111)$, with x = a for SO_2 and x = d for NO) vs the surface d-band center of the surfaces. M of each point is marked in the plot.

3.2.3. Estimation of $E^{TS}_{SO_2} - E^{IS}_{SO_2}$ *and* $E^{TS}_{NO} - E^{IS}_{NO}$. On the basis of the electronic composition−property relationships for SO_2 and NO at both initial states and transition states in the previous two subsections, the $E^{TS}_{SO_2} - E^{IS}_{SO_2}$ and $E^{TS}_{NO} - E^{IS}_{NO}$ values on different surfaces can be calculated. Figure 9 shows $E^{TS}_x - E^{IS}_x$ (x = SO_2 and NO) as functions of the weighted d-band center of surfaces. Note that the weighted d-band center model used in the previous two subsections incorporates the binding strength of atoms in adsorbates and metal surface atoms. It is therefore adsorbate dependent. Thus, we cannot simply subtract eqs 5 and 6 from eqs 7 and 9 in order to compare the barrier between the oxidation of NO and that of SO_2 on a given surface. Instead, we subtract E^{IS}_x (obtained from eqs 5 and 6) from E^{TS}_x (obtained from eqs 7 and 9) (x = SO_2 and NO) and then plot the energy differences as the function of the surface d-band center in Figure 9. Here, the surface d-band center is calculated as $(\sum_{x=a,b,c,d} E^x_d)/4$, where E^x_d represents the d-band center of surface atom x (x = a, b, c, or d, as marked in Figure 3). As can be seen in Figure 9, $E^{TS}_{SO_2} - E^{IS}_{SO_2}$ (dashed line) increases as the surface d-band center increases. $E^{TS}_{NO} - E^{IS}_{NO}$ (solid line) slightly decreases with an increase in the surface d-band center until it reaches ~ -2.22 eV. Once it reaches -2.22 eV, the slope of $E^{TS}_{NO} - E^{IS}_{NO}$ versus the surface d-band center changes dramatically. $E^{TS}_{NO} - E^{IS}_{NO}$ increases significantly as the surface d-band center shifts toward the Fermi energy level. Although the plot in Figure 9 is based on the single substitution of a surface Pt atom, double substitution has been tested and found to follow the same trend. As explained in section 3.1.2, the difference in the energy barriers of NO oxidation and SO_2 oxidation mainly comes from the difference in $E^{TS}_{SO_2} - E^{IS}_{SO_2}$ and $E^{TS}_{NO} - E^{IS}_{NO}$. Therefore, the different sensitivities between $E^{TS}_{SO_2} - E^{IS}_{SO_2}$ and $E^{TS}_{NO} - E^{IS}_{NO}$ to the weighted d-band center of alloy surfaces can be used to guide us to the design of the new selective, sulfur-resistant oxidation automotive catalysts by applying the design strategy introduced in section 3.1.1.

Using $E^{TS}_{SO_2} - E^{IS}_{SO_2}$ and $E^{TS}_{NO} - E^{IS}_{NO}$ on various surfaces, we can estimate the selectivity of those surfaces for the oxidation of NO. Figure 10 illustrates the selectivity for the oxidation of NO at 700 K as a function of the surface d-band center (same as those in Figure 9). The temperature 700 K is chosen because it is about the operating temperature of lean NO_x traps. The selectivity is defined as the ratio of the reaction rate for the oxidation of NO to that for the oxidation reaction of SO_2. The reaction rate is estimated as

$$\text{rate} = A \times \exp\left(-\frac{E_a}{RT}\right) \qquad (10)$$

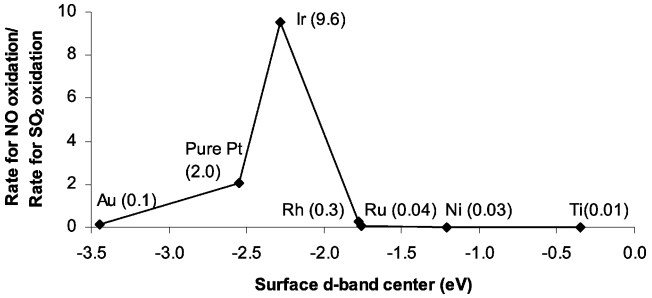

Figure 10. Plot of the rate ratio between the oxidation of NO and the oxidation of SO_2 at 700 K vs the surface d-band center of the surfaces ($1M^x$/Pt(111), with x = a for SO_2 and x = d for NO). M of each point is marked in the plot. Unit of y axis should be the prefactor ratio between the oxidation of NO and the oxidation of SO_2 at 700 K (AR).

where A is a constant prefactor, E_a is the energy barrier of the reaction, R is the ideal gas constant, and T is the temperature of the system. Therefore, the selectivity can be calculated by

$$\text{selectivity} = \frac{A_{\text{oxi-NO}} \times \exp\left(-\frac{E_{\text{oxi-NO}}}{RT}\right)}{A_{\text{oxi-SO}_2} \times \exp\left(-\frac{E_{\text{oxi-SO}_2}}{RT}\right)} \qquad (11)$$

Applying the energy barrier decomposition schemes in eqs 3 and 4 to eq 11, the selectivity in eq 11 can therefore be estimated as

$$\text{selectivity} = \frac{A_{\text{oxi-NO}} \times \exp\left(-\frac{E_{\text{NO}}^{\text{TS}} - E_{\text{NO}}^{\text{IS}}}{RT}\right)}{A_{\text{oxi-SO}_2} \times \exp\left(-\frac{E_{\text{SO}_2}^{\text{TS}} - E_{\text{SO}_2}^{\text{IS}}}{RT}\right)} \qquad (12)$$

For simplicity, we name the ratio of the prefactor for NO oxidation to that for SO_2 oxidation as AR. As shown in Figure 10, the highest selectivity (about 9.6AR) occurs at a surface d-band center value of −2.22 eV, which is very close to that of Ir alloyed Pt(111) surfaces. The selectivity for the oxidation of NO on a clean Pt(111) surface is about 2.0AR. All of the other surfaces (such as Au, Rh, Ru, Ni, or Ti alloyed surfaces) have a much lower selectivity (less than 0.3AR). Note that Mitsubishi Heavy Ind. in Japan has found that an Ir/metallosilicate catalyst works for the selective reduction of NO_x in lean burning gasoline engines.[36] The selectivity for the oxidation of NO over SO_2 also depends on the temperature. It is found to increase with the temperature decrease.

3.3. Validation of the Design Strategy by NEB Calculations. NEB calculations are carried out to validate the design strategy proposed in this paper and also to confirm the conclusions obtained from the composition−activity relationship illustrated in Figure 9. Au, Ir, and Rh alloyed surfaces are chosen as test systems, and their performance is compared to that of the clean Pt(111) surface. Double substitution for each alloy surface is used here. The minimum energy paths for the oxidation of SO_2 and NO on each surface are plotted in parts a and b of Figure 11, respectively. The geometry of images at each point along the MEP on alloy surfaces is found not to vary much from those on the clean Pt(111) surface. (Variation of bond lengths is less than 0.08 Å, and variation of bond angles is less than 6° in our calculations.) This is in agreement with the phenomena in Zhang et al.'s study of the oxidation of CO on $Cu_3Pt(111)$ alloy surfaces[33] and validates our assumption in section 3.1.2. The energy barriers of different reactions on each

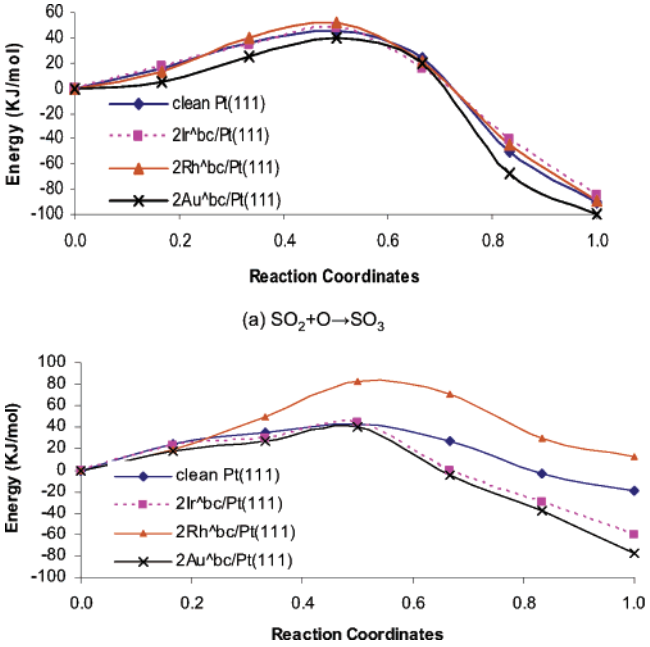

Figure 11. Minimum energy paths of the oxidation of (a) SO_2 and (b) NO on various alloyed Pt(111) surfaces found via NEB calculations.

TABLE 3: Energy Barriers, E_a, via NEB for the Oxidation of (a) SO_2 and (b) NO on Various Surface Alloys nM^x/Pt(111) and the Selectivity for Oxidation of NO at 700 K (Unit, AR; Prefactor Ratio of NO Oxidation to That of SO_2 Oxidation)

nM^x/Pt(111)	E_a for (a) (kJ/mol)	E_a for (b) (kJ/mol)	selectivity for (b) (%)
$2Au^{bc}$/Pt(111)	39.69	41.01	0.6
clean Pt(111)	45.66	43.52	1.4
$2Ir^{bc}$/Pt(111)	48.56	44.61	2.5
$2Rh^{bc}$/Pt(111)	51.32	83.34	0.01

surface are compiled in Table 3. As shown in Table 3, from $2Au^{bc}$/Pt(111) to clean Pt(111), to $2Ir^{bc}$/Pt(111), and to $2Rh^{bc}$/Pt(111), the energy barrier of $SO_2 + O \rightarrow SO_3$ increases slowly but steadily; however, the energy barrier of $NO + O \rightarrow NO_2$ remains more or less flat from $2Au^{bc}$/Pt(111) to clean Pt(111) and to $2Ir^{bc}$/Pt(111) and increases significantly on $2Rh^{bc}$/Pt(111). The values of the barriers in Table 3 show that the trend agrees with what we obtained from the composition−activity plot in Figure 9. The selectivity of NO oxidation is also calculated and given in the last column of Table 3. The alloy surface $2Ir^{bc}$/Pt(111) has the highest selectivity among those four tested surfaces, followed by the clean Pt(111) surface, which has a selectivity of around 1.4AR, in reasonable agreement with the selectivity curve in Figure 10, which is based on the composition−activity plot in Figure 9. The discrepancy between selectivity of NO oxidation on Au and Rh alloyed surfaces might be due to the simplifications of our model, but this would not keep us from observing the main trend shown in Figure 10 which is what we care about. Therefore, our selective, sulfur-resistant catalyst design strategy based on the composition−activity relationship is reasonably reliable.

4. Conclusions

We have proposed a new design strategy for catalysts based on correlating our recently developed modified d-band center model with reaction barriers on surfaces.[6,7] We have applied our approach to an important environmental application, the design of sulfur-resistant, lean NO_x catalysts for emissions

reduction from mobile sources. Specifically, we have aimed our design at finding a catalyst with maximum selectivity for oxidizing NO over SO_2. We found that an alloy surface with a surface d-band center around −2.22 eV (such as the Ir alloyed Pt(111) surface) has the highest selectivity for oxidation of NO (around 9.6AR). It was unfortunate, however, that the correlation of our modified d-band center with the transition state of NO + O had a change of slope, limiting the theoretical selectivity. Ongoing work aims at understanding the reasons for this. The design strategy proposed in this work is general and could be applied to other catalytic systems.

Acknowledgment. This work was supported in part by the National Science Foundation, CTS-9984301, and the Singapore-MIT Alliance.

References and Notes

(1) Gross, W. F. B. P.; Greene, D. F.; Kearby, K. K. U.S. Patent 3,370,914.
(2) Shelef, M. *Chem. Rev.* **1995**, *95*, 209.
(3) Takahashi, N.; et al. In *Proceedings of the First World Congress on Environmental Catalysis*, Pisa, Italy, May 1−5, 1995; Centi, C., Perathoner, S., Cristiani, C., Forzatti, P., Eds.; Societa Chimica Italiana: Rome; pp 45−48.
(4) Sachtler, W. M. H. *Le Vide* **1973**, *28*, 67.
(5) Besenbacher, F.; Chorkendorff, I.; Clausen, B. S.; Hammer, B.; Molenbroek, A. M.; Nørskov, J. K.; Stensgaard, I. *Science* **1998**, *279*, 1913.
(6) Tang, H.; Trout, B. L. *J. Phys. Chem. B* **2005**, *109*, 6948.
(7) Tang, H.; Trout, B. L. *J. Phys. Chem. B* **2005**, *109*, 17630.
(8) Hammer, B. *Phys. Rev. Lett.* **1999**, *83*, 3681.
(9) Burch, R.; Daniells, S. T.; Hu, P. *J. Chem. Phys.* **2002**, *117*, 2902.
(10) Shelef, M.; McCabe, R. W. *Catal. Today* **2000**, *62*, 35.
(11) http://www.fysik.dtu.dk/CAMP/dacapo.html.
(12) Perdew, J. P.; Chevary, J. A.; Vosko, S. H.; Jackson, K. A.; Pederson, M. R.; Singh, D. J.; Fiolhais, C. *Phys. Rev. B* **1992**, *46*, 6671.
(13) Vanderbilt, D. *Phys. Rev. B* **1990**, *41*, 7892.
(14) Laasonen, K.; Pasquarello, A.; Car, R.; Lee, C.; Vanderblit, D. *Phys. Rev. B* **1993**, *47*, 10142.
(15) Monkhorst, H. J.; Pack, J. D. *Phys. Rev. B* **1976**, *13*, 5188.
(16) Lin, X.; Schneider, W. F.; Trout, B. L. *J. Phys. Chem. B* **2004**, *108*, 250.
(17) Mavrikakis, M.; Hammer, B.; Nørskov, J. K. *Phys. Rev. Lett.* **1998**, *81*, 2819.
(18) Pallassana, V.; Neurock, M.; Hansen, L. B.; Nørskov, J. K. *J. Chem. Phys.* **2000**, *112*, 5435.
(19) Aizawa, H.; Morikawa, Y.; Tsuneyuki, S.; Fukutani, K.; Ohno, T. *Surf. Sci.* **2002**, *514*, 394.
(20) Lin, X.; Hass, K. C.; Schneider, W. F.; Trout, B. L. *J. Phys. Chem. B* **2002**, *106*, 12575.
(21) Alavi, A.; Hu, P.; Deutsch, T.; Silvestrelli, P. L.; Hutter, J. *Phys. Rev. Lett.* **1998**, *80*, 3650.
(22) Li, X.; Gewirth, A. A. *J. Am. Chem. Soc.* **2003**, *125*, 7086.
(23) Tang, H.; Van der Ven, A.; Trout, B. L. *Phys. Rev. B* **2004**, *70*, 045420.
(24) Kitchin, J. R.; Nørskov, J. K.; Barteau, M. A.; Chen, J. G. *Phys. Rev. Lett.* **2004**, *93*, 156801.
(25) Tsai, M.-H.; Hass, K. C. *Phys. Rev. B* **1995**, *51*, 14616.
(26) Hass, K. C.; Tsai, M.-H.; Kasowski, R. V. *Phys. Rev. B* **1996**, *53*, 44.
(27) Hammer, B.; Nørskov, J. K. *Phys. Rev. Lett.* **1997**, *79*, 4441.
(28) Jónsson, H.; Mills, G.; Jacobsen, K. W. Nudged Elastic Band Method for Finding Minimum Energy Paths of Transitions. In *Classical and Quantum Dynamics in Condensed Phase Silmulations*; Berne, B. J., Ed.; World Scientific: Singapore, 1998; p 385.
(29) Ulisky, A.; Elber, R. *J. Chem. Phys.* **1990**, *92*, 1510.
(30) Lin, X.; Schneider, W. F.; Trout, B. L. *J. Phys. Chem. B* **2004**, *108*, 13329.
(31) Liu, Z.; Hu, P. *J. Chem. Phys.* **2001**, *115*, 4977.
(32) Liu, Z.; Hu, P.; Lee, M. *J. Chem. Phys.* **2003**, *119*, 6282.
(33) Zhang, C. J.; Baxter, R. J.; Hu, P.; Lee, M. H. *J. Chem. Phys.* **2001**, *115*, 5272.
(34) Loffreda, D.; Simon, D.; Sautet, P. *J. Chem. Phys.* **1998**, *108*, 6447.
(35) Nilsson, A.; Pettersson, L. G. M.; Hammer, B.; Bligaard, T.; Christensen, C. H.; Nørskov, J. K. *Catal. Lett.* **2005**, *100*, 3−4.
(36) Nojima, S.; Iida, K.; Kobayashi, N. (Mitsubishi Heavy Ind., Japan) http://www.bsk.ynu.ac.jp/tatsumi/TOCAT4/poster.html (IP233).